Spatial inhomogeneities at the LaAlO₃/SrTiO₃ interface:
Evidence from second harmonic generation

T. Günter,[1] A. Rubano,[1] D. Paparo,[2,*] M. Lilienblum,[1] L. Marrucci,[2] F. Miletto Granozio,[2] U. Scotti di Uccio,[2] R. Jany,[3] C. Richter,[4] J. Mannhart,[4] and M. Fiebig[1,5]

[1]*HISKP, Universität Bonn, Nussallee 14-16, 53115 Bonn, Germany*
[2]*CNR-SPIN and Università di Napoli, Compl. Univ. di Monte S. Angelo, v. Cintia, 80126 Napoli, Italy*
[3]*Center for Electronic Correlations and Magnetism, Universitätsstrasse 1, University of Augsburg, 86135 Augsburg, Germany*
[4]*Max Planck Institute for Solid State Research, Heisenbergstrasse 1, 70569 Stuttgart, Germany*
[5]*Department of Materials, ETH Zurich, Wolfgang-Pauli-Strasse 10, 8093 Zurich, Switzerland*

Phase-sensitive, spatially resolved optical second-harmonic-generation experiments were performed on LaAlO₃/SrTiO₃ heterostructures. Lateral inhomogeneities on a length scale of ≈ 30 μm are found when a one-unit-cell-thick epitaxial monolayer of LaAlO₃ is grown on TiO₂-terminated SrTiO₃ single crystals. The inhomogeneity is absent in samples with LaAlO₃ layers of more than one unit cell. The results are discussed in the framework of electronic, oxidic, and chemical inhomogeneities.

I. INTRODUCTION: HOMOGENEITY OF LaAlO₃/SrTiO₃ INTERFACES

A quasi-two-dimensional electron gas is formed at the n-type LaAlO₃/SrTiO₃ interface when $n \geqslant 4$ monolayers of LaAlO₃ are deposited onto the SrTiO₃ substrate.[1] Since its discovery, the emergence of a conducting state between two insulating oxides has been attracting strong interest.[2,3] Quite soon, it was realized that the so-called *polar catastrophe scenario* describing an electrostatic breakdown[4] captures the mechanism driving the formation of the conducting state, but it does not give a complete picture of the underlying physics and phenomena. More detailed models have to account for the interfacial carrier density observed in Hall measurements,[3] which is found to be one order of magnitude lower than what is predicted by the polar catastrophe scenario, as well as for the distribution of oxygen vacancies[5] and for the stabilization of local inhomogeneities, such as a tip-induced conductivity.[6] Recently, optical second harmonic generation (SHG) revealed that the electronic reconstruction at the interface occurs at $n = 3$ with precursors at $n = 1,2$, while the onset of conductivity occurs in a separate step at $n = 4$. Aside from carrier-trapping scenarios, the occurrence of local inhomogeneities in the electronic structure of the interface was proposed as a possible reason for the delayed emergence of the conducting state.[7] This is supported by several theoretical and experimental works.[8–11] In addition, evidence for magnetic[12] and chemical[13] phase separation was reported. Yet the lateral spatial distribution of the interface reorganization in the LaAlO₃/SrTiO₃ system has been the topic of only a few reports so far.[12–15]

In this work, we investigate the electronic reconstruction in the LaAlO₃/SrTiO₃ system by spatially resolved SHG. We show that lateral polarization inhomogeneities on a length scale of ≈ 30 μm dominate the optical response of the LaAlO₃/SrTiO₃ interface at $n = 1$, whereas a much more homogeneous response is observed at $n \neq 1$, i.e., throughout the electronic redistribution and the conductivity changes. Possible reasons for the influence of the single LaAlO₃ overlayer on the interfacial polarization inhomogeneity are discussed.

II. PROBING LaAlO₃/SrTiO₃ INTERFACES BY SHG

SHG is a well established tool for studying polar asymmetries at the LaAlO₃/SrTiO₃ interfaces.[7,16] It describes the induction of a light wave of frequency 2ω by a fundamental light wave of frequency ω according to $P_i(\omega) = \epsilon_0 \chi_{ijk}^{(2)} E_j(\omega) E_k(\omega)$. The component $\chi_{ijk}^{(2)}$ of the nonlinear susceptibility tensor couples j- and k-polarized contributions of the incident light field to an i-polarized contribution of the SHG light field. In the electric-dipole approximation, $\chi^{(2)}$ is a polar tensor with $\chi_{ijk}^{(2)} \neq 0$ in noncentrosymmetric systems only.[7] Thus, SHG is ideal for investigating interfaces, because at interfaces the inversion symmetry is inherently broken. The SHG response integrates over the entire region in which the interface induces a polarization asymmetry. The bulk material that is not affected by the presence of the interface does not contribute to SHG. Here, by exploiting the *lateral* spatial degrees of freedom of SHG, we reveal the in-plane polar landscape of the interface.

III. SAMPLE PREPARATION

LaAlO₃/SrTiO₃ heterostructures were prepared by depositing LaAlO₃ on (001)-oriented and TiO₂-terminated SrTiO₃ substrates by pulsed laser deposition. The Ti-terminated SrTiO₃ substrates were prepared according to the procedure reported in Ref. 17: The purchased substrates were ultrasonically cleaned in demineralized water for 10 min and dipped for about 30 s into a commercially available buffered fluoridic acid solution. To facilitate surface recrystallization and remove any residual contamination, a final annealing step was performed at 950 °C for several hours in flowing oxygen. Note that the sample at $n = 0$, i.e., the bare STO substrate, was exposed to the same preparation cycle as the samples at $n > 0$.

Three batches of samples grown in Augsburg or Naples[7,16] were investigated under ambient conditions (air, 297 K). In all of them, the interfacial conduction emerges at $n = 4$, while samples with $n < 4$ were insulating. The growth process was monitored via reflection high energy electron diffraction
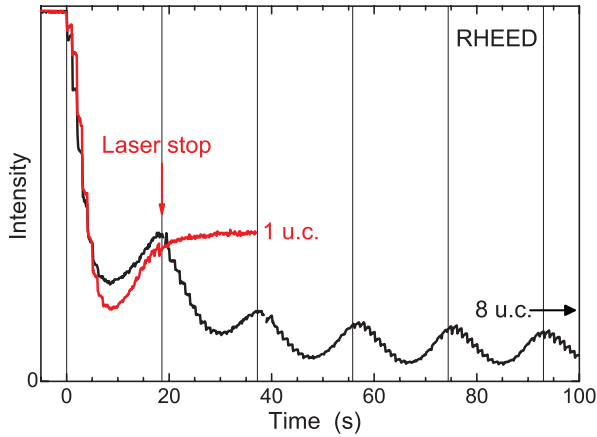
FIG. 1. (Color online) RHEED oscillations for the growth of $n = 8$ (black) and $n = 1$ (red) unit cells of $LaAlO_3$ on the TiO_2-terminated $SrTiO_3$ substrate. The growth process is calibrated with the help of the $n = 8$ sample, which reveals that 19 pulses complete a monolayer (vertical lines). In the subsequent growth of the $n = 1$ sample, the deposition is stopped after 19 pulses have been applied. The RHEED signal equilibrates at maximum intensity.

(RHEED) as shown in Fig. 1. Particular care was taken to ensure the completion of the sample at $n = 1$. At first, growth of a sample at $n > 1$ was used to calibrate the growth process. Figure 1 reveals that 19 laser pulses are required to complete one RHEED oscillation and, hence, one monolayer of $LaAlO_3$. Subsequently, the $n = 1$ sample was grown by stopping the deposition after 19 laser pulses. Comparison of the RHEED data taken during the $n = 1$ growth to those taken at $n > 1$ shows that this indeed completes the first monolayer.

The phenomena reported here were reproduced in all three batches, which highlights their robustness against growth-related differences and defects. Furthermore, all $LaAlO_3/SrTiO_3$ samples were prepared, treated, and investigated under identical conditions, which precludes external perturbations as a source of possible artifacts. Prior to the SHG experiments, the surfaces were cleaned with dry nitrogen gas without the use of adsorbates.[18] Note that the $n = 0$ samples were not exposed to the PLD environment anymore after pretests had shown that this exposure has no effect on the SHG signal and its spatial distribution.

IV. EXPERIMENTAL SETUP

Frequency-tunable laser pulses of 130 fs were generated at 1 kHz by an optical parametric amplifier pumped by a Ti:sapphire amplifier system. All SHG images were taken in a $90°$-reflection geometry at a SHG energy of 2.1 eV.[7] In the following, p (s) indicates a linear polarization parallel (perpendicular) to the plane of incidence. The samples were imaged by a liquid-nitrogen-cooled digital camera using either a telephoto lens (≈ 25 μm resolution) or a microscope lens (≈ 1 μm resolution).

V. EXPERIMENTAL RESULTS

Figure 2 shows two spatially resolved SHG images of $LaAlO_3/SrTiO_3$ heterostructures with $n = 1$ and 3. Note
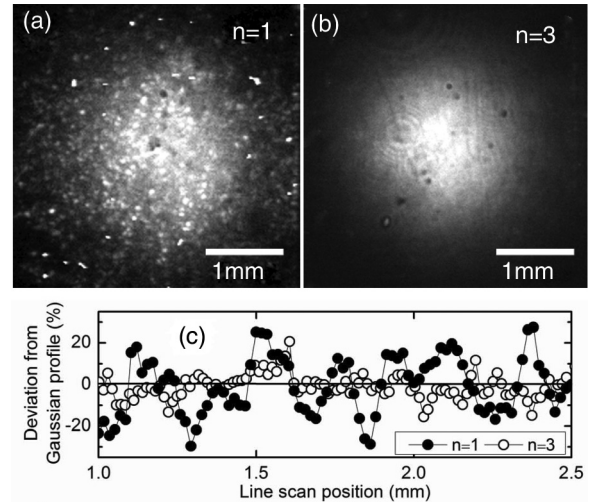

FIG. 2. (a,b) Spatially resolved SHG images of $SrTiO_3$ covered with n epitaxially grown monolayers of $LaAlO_3$. The images show the area illuminated with the Gaussian laser beam and are scaled to the respective minimum (black) and maximum (white) intensity. Resolution is 25 μm. (c) Deviation from Gaussian laser beam profile shown for typical horizontal line scans across the camera chip, vertically averaging across three neighboring pixels. The sample with $n = 3$ is chosen as representative for all the samples with $n \neq 1$. Lines are guides to the eye.

that aside from intensity changes [Fig. 3(b)], no qualitative difference between the images from samples with $n \neq 1$ was observed, so that only the sample with $n = 3$ is shown representatively. For better comparability, both images are scaled to the respective minimum (black) and maximum (white) intensity. A Gaussian laser beam profile is fitted to the intensity distribution in the images. Deviations from this profile are shown in Fig. 2(c) for a central horizontal cross section through the images in Fig. 2. The statistical variation of the data points in this kind of line scan, the inhomogeneity parameter, is shown in Fig. 3(a) as standard deviation, normalized to the value obtained for the bare $SrTiO_3$ substrate ($n = 0$).

For $n \neq 1$, deviations from the Gaussian beam profile are dominated by shot noise and defects or dust particles on the substrate or the camera. Neither the electronic reconstruction at $n = 3$ (with the related increase of the SHG intensity) nor the onset of conductivity at $n = 4$ affect the lateral homogeneity of the SHG signal. However, striking differences are found for $n = 1$ where we observe a blotchy distribution of the SHG intensity. The blotchiness is also evident in the line scan for $n = 1$ in Fig. 2(c) and in the normalized inhomogeneity parameter in Fig. 3(a). We see that the inhomogeneity parameter at $n = 1$ is about three times larger than for samples with $n \neq 1$. Reproducibility was verified for different samples with $n = 1$ (open data points) yielding a mean value of the corresponding inhomogeneity parameter of 3.35 ± 0.27, whereas a mean value of 1.25 ± 0.22 is obtained for samples with $n \neq 1$. In total, the blotchy SHG distribution was confirmed for four samples at $n = 1$ from different batches and laboratories, while the absence of inhomogeneities was verified for more than ten samples at $n \neq 1$. Not a single sample contradicted this pattern. In particular, no correlation to the interfacial transition around $n = 3$ [Fig. 3(b)] was found. Thus, the blotchy SHG
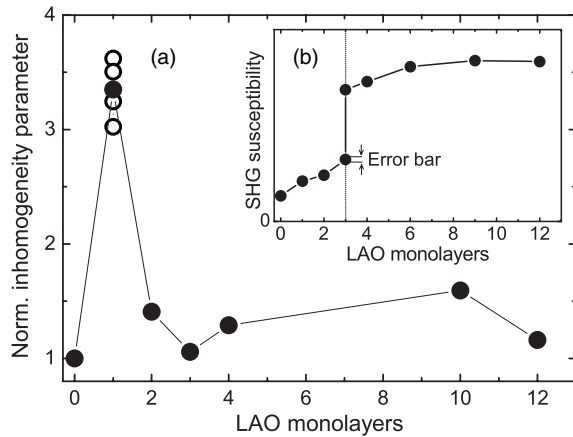
FIG. 3. (a) Inhomogeneity parameter describing the statistical variation of SHG intensity in line scans as in Fig. 2(c) for different values of n, normalized to $n = 0$. Reproducibility is confirmed by values obtained on other samples at $n = 1$ (open symbols). (b) Polarization-averaged SHG susceptibilities for different values of n show that the abrupt change of SHG yield at $n = 3$ and the precursor behavior in the vicinity of $n = 3$ have no effect on the inhomogeneity parameter. Lines are guides to the eye.

distribution is a robust and exclusive feature of $SrTiO_3$ covered with a single monolayer of $LaAlO_3$.

Often, speckles as in Fig. 2(c) indicate interfering SHG contributions from regions with a lateral extension below the resolution limit.[19] To determine the actual extension of these regions, we took high-resolution images of the $n = 1$ samples, such as the one shown in Fig. 4(a). With the resolution increased from 25 to 1 μm, we see that the SHG intensity varies steadily across about 30 μm, which is thus the "inhomogeneity length scale" of the $n = 1$ samples. It is found in all the $n = 1$ samples, but not in the samples with $n \neq 1$. [Note that the remaining sub-μm graininess of Fig. 4(a) does not indicate another substructure. It is found in all samples and caused by diffuse reflection of the SHG light off the matted $SrTiO_3$ rear side.]
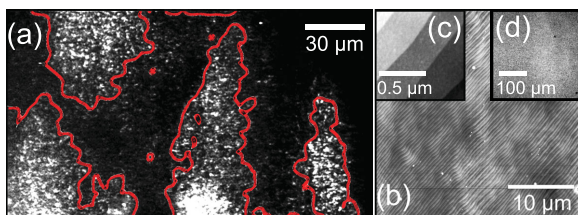

FIG. 4. (Color online) (a) High-resolution (1 μm) SHG image of a $LaAlO_3/SrTiO_3$ heterostructure at $n = 1$. The 50% contour lines show that the "inhomogeneity length scale" of the sample is about 30 μm. The grainy substructure of the image is explained in the text. (b,c) Typical AFM images of the same sample show a perfectly flat $SrTiO_3$ surface with substrate steps. The step height corresponds to one unit cell of the $SrTiO_3$ substrate. The long-range fluctuation of brightness in panel (b) is caused by a known artifact of the scanning process related to nonlinearities of the piezoelectric scanner of the AFM. It is not caused by structural variations across the surface, as is furthermore evidenced by the straight parallel monolayer steps which are still clearly recognizable. (d) No micrometric inhomogeneities are revealed by linear optical light microscopy.
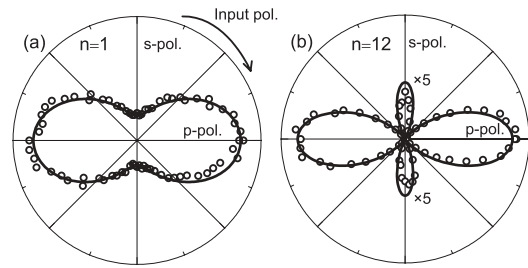

FIG. 5. Intensity of p-polarized contributions to the SHG signal as a function of the polarization of the incident fundamental light for $LaAlO_3/SrTiO_3$ heterostructures with (a) $n = 1$ and (b) $n \neq 1$, here represented by the sample with $n = 12$. Note that the s-polarized lobes in panel (b) are magnified by a factor 5.

Often the *phase*, aside from the *intensity*, of the SHG signal carries important information on spatial inhomogeneities such as domains. To understand the origin of the regions resolved in Fig. 4(a), we therefore performed a phase-sensitive polarization analysis of the SHG signal. In Fig. 5, we show the polarization dependence of the SHG signal for samples with $n = 1$ and 12. It was obtained by rotating the polarization of the incident light while detecting the p-polarized contribution to the SHG light. The fits for $n = 1$ and 12 show that for both samples, the polarization dependence can be described by the SHG tensor components $\chi_{ijk}^{(2)}$ allowed for the cubic 4 mm symmetry of the $LaAlO_3/SrTiO_3$ interface.[7] However, the fit for the sample with $n = 1$ requires *complex* values for $\chi_{ijk}^{(2)}$, whereas *real* fit parameters are sufficient for $n = 12$ (and any other sample with $n \neq 1$, not shown here). This constitutes the presence of a substructure on a macroscopic length scale in the $n = 1$ samples where regions differ primarily in the phase of the corresponding SHG light wave. In particular, the absence of new tensor components $\chi_{ijk} \neq 0$ shows that in spite of the inhomogeneities, the interfacial symmetry in the $n = 1$ samples remains at 4 mm: There are no indications of a deviation from the cubic crystallographic phase.

It may be argued that crystallographic defects of the substrate may cause the inhomogeneity revealed by the SHG images. However, aside from the presence of substrate steps, the atomic force microscope (AFM) scans in Figs. 4(b) and 4(c) reveal an atomically flat $SrTiO_3$ surface. This was verified in large-area AFM scans ($100 \times 100 \mu m^2$, not shown here) and at different positions on the sample. Likewise, *linear* optical microscopy measurements [Fig. 4(d)] did not yield micrometric inhomogeneities. The RHEED oscillations (examplarily shown in Fig. 1) do not show any indications that the first $LaAlO_3$ monolayer grows in a different quality or homogeneity than the following monolayers. We thus conclude that the topography of the $SrTiO_3$ substrate and the $LaAlO_3$ film is *not* responsible for the inhomogeneity of the $n = 1$ samples.

VI. DISCUSSION

In the following, we will review a variety of mechanisms that are known to cause spatial and SHG phase inhomogeneities, and we discuss to what extent they can be responsible for the inhomogeneities observed here in the $LaAlO_3/SrTiO_3$ system.

A. Electronic inhomogeneity

Many oxides are considered to be intrinsically electronically inhomogeneous at the nanoscale.[20] The presence of any distortions or defects induced during the growth process may alter the electronic properties of the material in a nonlinear way. For example, in manganites, theoretical studies that explicitly consider long-range effects, such as Coulomb forces between the electrons[21] or cooperative oxygen octahedra distortions,[22] show that even a very low degree of disorder can induce phase inhomogeneities. In $SrTiO_3$, cooperative polar distortions coupling directly to SHG can occur at a very low energetic cost as a consequence of its quantum-paraelectric nature.[23] Defects may produce long-range strain fields that affect the homogeneity of the polarization at length scales determined by the range of variation of the strain field. In some manganites, it has been shown that this scale may reach tens of microns,[24] comparable to what we report in this work. Thus, how could electronic effects explain the phase inhomogeneity observed here in the $LaAlO_3/SrTiO_3$ system? According to Ref. 25, the electrostatic potential at the interface leads to a competition between charge injection and polar distortions right from the deposition of the first monolayer of $LaAlO_3$. In agreement with Fig. 3(b), the polar distortion (and with it the SHG yield) increases until charge injection finally occurs. It is quite possible that at $n = 1$, the polar distortion is still so weakly manifested that it does not occur uniformly but breaks down into differently oriented regions instead. This can lead to a spatial variation of the phase,[26] or of the phase *and* the amplitude, of the SHG wave. Deposition of an additional $LaAlO_3$ layer strengthens the polar distortion and would therefore support a uniform polar distortion. This scenario agrees well with our observations, but independent evidence is required to establish it.

B. Oxidic inhomogeneity

Defects, such as oxygen vacancies, are a fundamental ingredient of the physics of complex oxides. If an inherent driving force triggers a clustering of the defects during the deposition of the first layer of $LaAlO_3$, a lateral inhomogeneous distribution can be expected, leading to the observed inhomogeneities. However, an interpretation in terms of defect clustering inevitably implies that the clustering disappears with the deposition of additional monolayers of LAO, thus resulting in the homogeneous distribution of SHG intensity that we observe. This is a very arbitrary assumption, especially since oxygen vacancies continue to persist independent of the thickness of the $LaAlO_3$ layer. Hence, this scenario is unlikely.

C. Chemical inhomogeneity

Aside from oxygen vacancies, chemical variations across the sample are a possible source for the formation of inhomogeneities. First, the chemical composition is well known to affect the phase of a SHG signal.[27] Second, experiments by Kelvin probe force microscopy and medium-energy ion spectroscopy were interpreted in terms of a formation of micrometer-sized regions with different La stoichiometry at the $LaAlO_3/SrTiO_3$ interface.[13] The authors concluded that La-doped areas in $SrTiO_3$ can provide stable nucleation sites promoting the formation of a stoichiometric $LaAlO_3$ film. Furthermore it is known that for thin $LaAlO_3$ films, La-Sr intermixing compensates for the interfacial dipole energy, thus avoiding an abrupt interface as experimentally observed in interdiffusion patterns of the $SrTiO_3$ substrate.[4,28] An inhomogeneous interdiffusion pattern may thus lead to the spatial inhomogeneities revealed by SHG. However, the details of such a mechanism, including the question of its restriction to the case of $n = 1$, would have to be clarified in order to establish it.

Among the options discussed in Secs. VI A, VI B, and VI C, we may thus favor electronic effects as being responsible for the polar inhomogeneity of the $n = 1$ sample, and we may exclude a scenario based on a clustering of oxygen defects. In any case, independent experiments are required to go beyond this very general discussion of mechanisms.

VII. CONCLUSION

In summary, we have observed lateral inhomogeneities at the interface between a $SrTiO_3$ substrate and a single monolayer of $LaAlO_3$ by means of spatially resolved optical SHG. The inhomogeneous interface state is a transient one that disappears once the second monolayer of $LaAlO_3$ is deposited. The inhomogeneities are characterized by the formation of regions with a lateral extension of ≈ 30 μm. A general discussion of possible mechanisms favors electronic effects, considers the involvement of chemical inhomogeneities, but discards an involvement of oxygen defects. Independent experiments are required to further highlight this matter and are anticipated by presenting our observations in this work.

*domenico.paparo@spin.cnr.it

[1] A. Ohtomo and H. Y. Hwang, Nature (London) **427**, 423 (2004).

[2] S. Thiel, G. Hammerl, A. Schmehl, C. Schneider, and J. Mannhart, Science **313**, 1942 (2006).

[3] A. D. Caviglia, S. Gariglio, N. Reyren, D. Jaccard, T. Schneider, M. Gabay, S. Thiel, G. Hammerl, J. Mannhart, and J.-M. Triscone, Nature (London) **456**, 624 (2008).

[4] N. Nakagawa, H. Y. Hwang, and D. A. Muller, Nat. Mater. **5**, 204 (2006).

[5] Y. Chen, N. Pryds, J. E. Kleibeuker, G. Koster, J. Sun, E. Stamate, B. Shen, G. Rijnders, and S. Linderothl, Nano Lett. **11**, 3774 (2011).

[6] Y. Xie, C. Bell, T. Yajima, Y. Hikita, and H. Y. Hwang, Nano Lett. **10**, 2588 (2010).

[7] A. Rubano, M. Fiebig, D. Paparo, A. Marino, D. Maccariello, U. Scotti di Uccio, F. Miletto Granozio, L. Marrucci, C. Richter, S. Paetel, and J. Mannhart, Phys. Rev. B **83**, 155405 (2011).

[8] R. Pentcheva and W. E. Pickett, Phys. Rev. B **74**, 035112 (2006).

[9] Z. S. Popovic, S. Satpathy, and R. M. Martin, Phys. Rev. Lett. **101**, 256801 (2008).

[10] B. R. K. Nanda and S. Satpathy, Phys. Rev. B **83**, 195114 (2011).

[11] Ariando, X. Wang, G. Baskaran, Z. Q. Liu, J. Huijben, J. B. Yi, A. Annadi, A. Roy Barman, A. Rusydi, S. Dhar, Y. P. Feng, J. Ding, H. Hilgenkamp, and T. Venkatesan, Nat. Commun. **2**, 188 (2011).

[12] J. A. Bert, B. Kalisky, C. Bell, M. Kim, Y. Hikita, H. Y. Hwang, and K. A. Moler, Nat. Phys. **7**, 767 (2011).

[13] A. S. Kalabukhov, Y. A. Boikov, I. T. Serenkov, V. I. Sakharov, V. N. Popok, R. Gunnarsson, J. Börjesson, N. Ljustina, E. Olsson, D. Winkler, and T. Claeson, Phys. Rev. Lett. **103**, 146101 (2009).

[14] D. F. Bogorin, C. W. Bark, H. W. Jang, C. Cen, C. M. Folkman, C. B. Eom, and J. Levy, Appl. Phys. Lett. **97**, 013102 (2010).

[15] S. A. Pauli, S. J. Leake, B. Delley, M. Björck, C. W. Schneider, C. M. Schlepütz, D. Martoccia, S. Paetel, J. Mannhart, and P. R. Willmott, Phys. Rev. Lett. **106**, 036101 (2011).

[16] A. Savoia, D. Paparo, P. Perna, Z. Ristic, M. Salluzzo, F. Miletto Granozio, U. Scotti di Uccio, C. Richter, S. Thiel, J. Mannhart, and L. Marrucci, Phys. Rev. B **80**, 075110 (2009).

[17] G. Koster, B. Kropman, G. Rijnders, D. Blank, and H. Rogalla, Appl. Phys. Lett. **73**, 2320 (1998).

[18] Y. Xie, Y. Hikita, C. Bell, and H. Y. Hwang, Nat. Commun. **2**, 494 (2011).

[19] M. Fiebig, D. Fröhlich, T. Lottermoser, and M. Maat, Phys. Rev. B **66**, 144102 (2002).

[20] V. B. Shenoy, D. D. Sarma, and C. N. R. Rao, Chem. Phys. Chem. **7**, 2053 (2006).

[21] J. Schmalian and P. G. Wolynes, Phys. Rev. Lett. **85**, 836 (2000).

[22] J. Burgy, A. Moreo, and E. Dagotto, Phys. Rev. Lett. **92**, 097202 (2004).

[23] T. Günter, E. Bousquet, A. David, P. Boullay, P. Ghosez, W. Prellier, and M. Fiebig, Phys. Rev. B **85**, 214120 (2012).

[24] D. D. Sarma, D. Topwal, U. Manju, S. R. Krishnakumar, M. Bertolo, S. La Rosa, G. Cautero, T. Y. Koo, P. A. Sharma, S.-W. Cheong, and A. Fujimori, Phys. Rev. Lett. **93**, 097202 (2004).

[25] R. Pentcheva and W. E. Pickett, Phys. Rev. Lett. **102**, 107602 (2009).

[26] D. Meier, M. Lilienblum, P. Becker, L. Bohatý, N. A. Spaldin, R. Ramesh, and M. Fiebig, Phase Trans., doi: 10.1080/01411594.2012.696116.

[27] Y. Tanabe, M. Muto, M. Fiebig, and E. Hanamura, Phys. Rev. B **58**, 8654 (1998).

[28] S. A. Chambers, M. H. Engelhard, V. Shutthanandan, Z. Zhu, T. C. Droubay, L. Qiao, P. V. Sushko, T. Feng, H. D. Lee, T. Gustafsson, E. Garfunkel, A. B. Shah, J.-M. Zuo, and Q. M. Ramasse, Surf. Sci. Rep. **65**, 317 (2010).